The effect of B and Si additions on the structural and magnetic behaviour of Fe-Co-Ni alloy prepared by high-energy mechanical milling

N. Khitouni[a,b], R. Daly[a], L. Escoda[b], N. Llorca-Isern[c], J. J. Suñol[b], M. Khitouni[a], M. Dammak[a]

[a]Laboratory of Inorganic Chemistry, LR17ES07- Faculty of Sciences of Sfax, University of Sfax, Tunisia

[b]Dep. of Fisica, University of Girona, Campus Montilivi, Girona, Spain

[c]Dept. CMEM, University of Barcelona, Martí Franquès 1, 08028 Barcelona, Spain

Abstract:

We investigate the structural and magnetic properties of nancrystalline $Fe_{50}Co_{25}Ni_{15}X_{10}$ ($X=B_{amorphous}$, $B_{crystalline}$ and Si) alloy powders prepared by mechanical alloying process. Morphological, microstructural and structural characterizations of the powders milled several times were investigated by scanning electron microscopy and X-ray diffraction. The final metallurgical state strongly depends on the chemical composition and the grinding time; it can be single-phase or two-phase. The crystallite size reduction down the nanometer scale is accompanied by the introduction of high level of lattice strains. The dissolution of Co, Ni, B (amorphous and crystalline) and Si into the α-Fe lattice leads to the formation of highly disordered Fe-based solid solutions. Coercivity (Hc) and the saturation magnetization (Ms) of alloyed powders were measured at room temperature by a vibration sample magnetization. The magnetic measurements show a contrasting Ms and (Hc) in all alloy compositions. Conclusively, soft magnetic properties of nanocrystalline alloys are related to various factors such as metalloids addition, formed phases and chemical compositions.

Keywords: Mechanical alloying; Fe-Co-Ni alloy; Microstructure; Magnetic properties.

1. Introduction

Significant efforts were made to improve the strength and resistivity of iron through development of nanomaterials and alloying additions. Mechanosynthesis is among the techniques that favors the formation of nanocrystalline and/or amorphous iron alloys after a sufficient milling time [1-2]. Further, the release of residual stress generated during milling process, tend to lead to better magnetic properties, including higher saturation magnetization (Ms) and lower coercivity (Hc)..Fe-Co alloys are also known as soft magnetic materials [3,4]. The great effect of the addition of a third element (Ni, Cu, V, Mo, Sn) on the mechanical and magnetic properties of the Fe-Co system are also examined in detail [5-10]. On the other hand, the addition of certain amount of metalloids, in particular C, B, Si and P favors thermal stability and the soft magnetic properties of Fe-based alloys [11]. Moreover, the addition of small amounts of boron to alloys can modify the fracture mode from intergranular failure to transgranular fracture by being segregated to grain boundaries. Studies on the microstructure of these alloys gave evidence that the addition of boron can also result in the formation of Fe_2B precipitates and a tetragonal phase which is likely coherent with the matrix [12]. Boron has been also found to facilitate the development of amorphous and nanocrystalline structures in the bcc-Fe phase [13]. Alternatively, Liu et al. [14] pointed out that the addition of 6 wt % Si to Fe-30Mn alloy rendered a material with shape memory effect and better corrosion performance. The addition of Si increases the resistivity leading to decrease in core losses in Fe-Si alloy [15,16]. In the present work we have selected the $Fe_{50}Co_{25}Ni_{25}$ compound as the starting alloy, and we have explored what changes are induced on the microstructure by the addition of 10 at. % $B_{amorphous}$, 10 at. % $B_{cristalline}$ and 10 at. % Si. Besides, the variation of the room temperature magnetic properties with the B and Si contents are reported.

2. Materials and methods

The mixtures of $Fe_{50}Co_{25}Ni_{15}X_{10}$ (X=$B_{amorphous}$, $B_{crystalline}$ and Si) (at.%) powders were prepared in proportions corresponding to the nominal composition from the elemental powders of Fe (99.97% purity, mean particle size < 10 μm), Co (99.9% purity, mean particle size < 2-5 μm), Ni (99.7 % purity, mean particle size < 10 μm), $B_{cristalline}$ (purity> 99%), $B_{amorphous}$ (purity> 99.5) and Si (99.5 % purity, mean particle size < 10 μm) by using a high-energy planetary ball-mill (Type P7) under Ar atmosphere. Ball milling experiments were carried out in a hardened steel container. The ball-to-powder weight ratio (Q) is 2:1 and the milling speed (ω) was adjusted to 600 rpm. Different milling times ranging from 0 to 100 h were used. The milling sequence was selected such as 10 minutes of milling followed by 5 minutes of idle period, to prevent sticking of the powder to container walls and the balls, and powder agglomeration during milling.X-ray diffraction (XRD) measurements were done using a D-500 Siemens equipment with CuK_{α} radiation. The size of the crystallites, the lattice strains and lattice parameter were calculated based on the Rietveld method using the Maud program [17]. In all refined XRD patterns, refinement parameter R_{exp} is lower than 10.5% and GOF parameter lower than 1.6. The morphology and the composition of mechanically alloyed powders were examined by scanning electron microscopy (SEM) in a DSM960A ZEISS microscope in secondary electron mode operating at a voltage of 15 kV. The SEM was equipped with a Vega_Tescan energy dispersive X-ray spectrometry (EDS) analyzer. The magnetic characterization was carried out by Superconducting Quantum Interference Device from Quantum Design SQUID MPMS-XL at 300 K (about 150 mg of powder in each experiment).

3. Results and discussion

3.1.Morphology

Figure 1 shows the microstructure of the $Fe_{50}Co_{25}Ni_{25}$, $Fe_{50}Co_{25}Ni_{15}B_{10(amorphous)}$, $Fe_{50}Co_{25}Ni_{15}B_{10(crystalline)}$ and $Fe_{50}Co_{25}Ni_{15}Si_{10(amorphous)}$ before milling (Fig. (1 a-d)) and after

mechanical milling for 50 h (Fig.(1 a1-1d1)) and 100 h (Fig.(1 a2-1d2)). It can be seen that increasing the milling time from 0 to 100 h results in a considerable reduction in the particle size of all the powder. After an intermediate time of 50 hours milling, the shape distribution of all the compositions and powders shows larger particles of irregular shape and size due to cold welding (Fig. 1 a1-d1). Depending on the dominant compressive forces, the particle size either may become smaller (relatively fine particles) due to fracturing, or larger (agglomerated particles) by cold welding during the grinding process. Indeed, the work-hardening due to these compressive forces of the milling causes a hardening of the powder particles and consequently leads to their fracture. The atomically clean surfaces created during fracture allow the particles to be welded again, which increases the size of the particles. In addition, it can be noted that the size of the particles depends on the nature of added metalloid; the size increases from the sample free of metalloid to the rich in amorphous boron, the crystallized boron and the silicon. This may be related partly to the nature of the starting particles because the presence of B and Si increases the hardness and brittleness of the powders. As a result, relatively hard particles tend to resist attrition and compressive forces and therefore,may remain less deformed. Si-rich powder has the largest particle size. Finally, as shown in Fig. 1a2-d2, the morphology of the particles obtained after milling for 100 h becomes finer and more homogeneous. In fact, increasing deformation and work hardening disintegrate the agglomerated powders into fragments, giving rise to a fine particle size distribution. On the other hand, at this more advanced stage of milling, B and Si can help in refining the morphology. This effect could be due to the preferential diffusion of B and Si atoms to the interstitial sites of the bcc phase through grain and particle boundaries enhancing the precipitation of Fe-B and Fe-Si compounds there. This phenomenon has a beneficial effect on the fracture mode of FeCoNi alloys, which changes from intra-granular to inter-granular

fracture mode. These observations suggest that the presence of the fracture surfaces can be associated with the presence of borides and silicon-rich phases in grain boundaries.

3.2. Structural properties

As the milling time increases, the X-ray diffractograms show an expansion of the different diffraction peaks and a decrease in their intensities. This behavior is a characteristic common to powders prepared by high-energy mechanical milling [1, 2]. The broadening of the diffraction peaks can be attributed to (i) the finite dimension of the diffracting domains in a coherent way and/or (ii) the structural imperfections able to distort the crystal lattice and then to cause a variation of inter-reticular distances around a mean value. Thus, a slight displacement is observed which is not the same for all the diffraction peaks and milling times. The displacement of a peak comes from the formation of a solid solution by mechanical milling and the introduction during the milling process of the first-order stresses acting on the macroscopic scale by modifying the lattice parameter of the material. Figure 2 shows the XRD patterns obtained of the milled samples with different metalloids addition as function of milling time. In the starting powders, all the major XRD peaks were found to correspond to that of bcc-Fe (SG Im-3m; a = 2.866 Å), hcp-Co (SG P63/mmc; a = 2.500 Å and c = 4.140 Å) and fcc-Ni (SG Fm-3m; a=3.523 Å) and fcc-Si (SG Fd-3m; a=5.4309 Å) elements as the B used was amorphous or crystalline with a low atomic scattering factor and did not therefore contribute to any significant peaks in the diffraction patterns. For the sample without metalloid addition, the small shift of the main diffraction peak (110) of α-Fe after 50h of milling can be related to the lattice variation due to distribution of Co and Ni atoms in the lattice of Fe resulting in the formation of supersaturated solid solution bcc-Fe(Co,Ni) (SG Im-3m; a = 2.8380(1) Å). After 100 h of milling, one can notice the appearance of new diffraction peaks, on the lower angle side of hcp-Co ones, due to the formation of the fcc-Co solid solution. This can be explained by the allotropic transformation of hcp-Co to fcc-Co. It

has been suggested that the hcp-Co phase becomes unstable when an external mechanical energy is introduced [18-20]. For the other samples containing metalloids B and Si, this phase transition hcp-Co → fcc-Co has been noticed only for amorphous boron addition after 10 h milling (Fig. 2b), but it disappears after 50 h. The boron doped samples (in its two states) showed that its dissolution in the iron lattice led to the appearance of new phases of boride type such as cubic-$Fe_{23}B_6$, tetragonal-FeB, tetragonal-Fe_2B and orthorhombic-Fe_3B. Indeed, in the case of sample with amorphous boron (Fig. 2b), one can notice the rapid formation of cubic-$Fe_{23}B_6$ phase. This phase adopts the $Cr_{23}C_6$ prototype structure with the Fm3m space group. This metastable phase can easily decompose into Fe_3B and Fe_2B. However, when the Fe atom site is partially substituted by another transition metal atom such as Co, or Ni, the phase is stabilized and more easily retained [21]. The formation of bcc-Fe(Co) and Fe (Ni) solid solutions was also noticed in this stage. The increase of the main α-Fe diffraction peak intensity after 12 h of milling in comparison with that of 6 h (Fig. 2) as well as the formation of the Fe_3B type boride (SG Pnma; a=5.406 Å, b=6.661 Å and c=4.363 Å) can be correlated to the decomposition of the $Fe_{23}B_6$ type boride through the following reaction: $Fe_{23}B_6 \rightarrow 5Fe + 6Fe_3B$ [22]. The obtained products at milling time superior to 25 h consists of a highly disordered Fe(Co,Ni,B) solid solution and Fe_3B boride phase with relative proportions (calculated by Rietveld) of about 83 and 17%, respectively (Fig. 2b). On the other hand, the B crystalline atoms substitute Fe atoms in bcc-Fe(B) solid solution, which will result in a decrease of the lattice parameter and therefore in a slight shift of the main (110) diffraction peak of α-Fe. This phase coexists with a bcc-Fe(Co) phase up to 25 h milling. The complete disappearance of Co, Ni diffraction peaks above 25 h of milling can be due to completion of bcc- Fe(Co,Ni,B) solid solution formation which is accompanied by the relaxation of lattice contraction. Therefore, the line profiles become symmetric (Fig. 2c).

In the case of the FeCoNiSi sample, the fcc-Ni(Si) solid solution which nucleated after 17 h with a proportion of 33%, persists up to a milling of 50 h (Fig. 2d). While the appearance of Fe(Co) solid solution was at 6 h milling and its disappearance was noted at 50 h. After 100h milling FeCoNiSi sample showed the complete dissolution of Co, Ni and Si in Fe lattice and the obtained powder consists of a highly disordered bcc-Fe(Co, Ni, Si) solid solution.

There was a slight shift in the XRD peaks of Fe towards lower or higher Bragg angle reflecting a level of increase or decrease in the lattice parameter with increasing milling time. Figure 3 shows the variation of the lattice parameter of each of the four samples without and with metalloid as a function of the milling time. Before 17 h of milling, unlike the doped samples, the lattice parameter of FeNiCo sample decreases progressively as a function of the milling time. This can be explained by the effect of severe plastic deformation, which predominates that of the solid solution, which can cause compression of the crystal lattice. For the doped samples, one can notice a certain irregularity in the evolution of the lattice parameter related to the dissimilar contribution of boron and silicon. However, the presence of B and Si in Fe lattice increases the hardness and brittleness of the powders making the deformation of the lattice more difficult. Further, the increase in the lattice parameter may be associated with the effect of solid solution of substitution and insertion. Since Co (1.52 Å) and Ni(1.49 Å) atomic radius are larger than Fe atomic radius (1.26 Å), their dissolutions next to metalloids B(0.87 Å) and Si(1.11 Å) into Fe matrix increased the lattice parameter of bcc α-Fe phases. Furthermore, the increase of the density of the defects during milling can give rise to an increase of the lattice parameter. On the other hand, the crystallite size and the level of lattice strains are very important because the formation of solid solutions and the transformation characteristics depend on them. Further milling results in a slight decrease in the lattice parameter. This can probably be related to crystal expansion due to the high concentration induced by structural defects (dislocations, point defects, gaps ...). For example,

the solution of point defects in the crystal lattice will disrupt its structure around the vacant positions ultimately leading to a distorted crystal lattice. The latter becomes more significant with smaller crystallites and promotes a higher solubility of the vacancies [23]. On the other hand, it is interesting to note that in the final milling products the lattice parameter increases from the FeCoNi to FeCoNiSi, $FeCoNiB_{amorpous}$ and $FeCoNiB_{crystalline}$.

The dependence of the calculated crystallites size and microstrains on milling time of the as-milled powders is given in Figure 4. It is clear that the crystallite size decreased with an increase in the milling time for all alloys (Fig. 4a; Table 1). However, the crystallite size of FeCoNiSi powder drastically decreased during the first twenty hours approximately to 37±2 nm. Increasing the milling time to 100 h, the size reaches to 10±2 nm. For the doped alloy with boron, the crystallite size for a $FeCoNiB_{crystalline}$ powder appears thinner than $FeCoNiB_{amorpous}$. The size differences for 25 and 100 h milling are calculated on the order of 25 and 40 nm, respectively. On the other hand, the crystallites size of FeCoNi powder has approximately the average values from that of the alloys doped with boron, especially for advanced grinding times. At the same time, the lattice strain increases with milling time (Fig. 4b). As expected, it increases with increasing of milling time more rapidly at the beginning and with slower trend at longer milling times. After 25 h milling, values of the lattice strain for the Si-doped alloy are relatively high compared to that of other powders, while the lowest values are identified for the $B_{amorphous}$-doped alloy. However, the evolution of lattice strain as a function of milling time for FeCoNi and $FeCoNiB_{crystalline}$ alloys are similar and the values reached after 100 h are around of 0.9%. These differences in lattice strain can be associated with the segregation of boron atoms and silicon in grain boundaries, which avoids the crystallite growth of the bcc phase. In addition, the instability in the segregation process can be explained by the increasing of the crystallites size and the decreasing of internal stresses during milling. The increasing of residual strains inside the material could be due to stress

field associated with the multiplication of the dislocations. Micro-stress in crystallites is generated by defects. It is worth to note that the reduction in crystallite size is accompanied by an increase in the lattice strain level as the MA time increases. This is a common behavior for all metallic systems prepared by MA.

3.1. Magnetic properties

The microstructures obtained after mechanical milling can strongly influence the magnetic properties of alloys [24]. The time dependence of the hysteresis loops at 300K, of the mechanically alloyed FeNiCo, $FeNiCoB_{amorphous}$, $FeNiCoB_{crystalline}$ and FeNiCoSi powder mixtures for selected milling times are shown in Fig.5. All hysteresis cycles exhibited a sigmoidal shape, which is usual in nanostructured samples with small magnetic domains [22]. This is due to the presence of structural distortions inside the grains. The small hysteresis losses are properties generally desired in soft magnetic materials. Fig. 6 presents the influence of metalloid additions on coercivity (Hc) and its dependence with milling time. It is noteworthy that the evolution of Hc can be divided into three stages for the doped alloys and in two stages for the undoped one : an ascending part for advanced milling times below of 6 h followed by a descent for times up to 50 h milling for all alloys, while for higher times there is an increase in the Hc value which intensifies from doped alloys by boron to that doped by Si; At the end of milling we note Hc values of 50 Oe for $FeCoNiB_{amorphous}$, 59 Oe for $FeCoNiB_{crystalline}$ and 90 Oe for FeCoNiSi). For the undoped alloy the Hc continues to decrease until the end of milling to reach a value of 12.5 Oe. On the basis of these Hc values, the B and Si-doped samples can be classified as semi-hard magnets (12.6 Oe < Hc <2.5 KOe), while the undoped sample can be considered like a soft magnet (Hc < 12.6 Oe). The increase of Hc can be attributed to the introduction of internal stresses and structural defects such as dislocations.Since the dislocations distort the surrounding material, stress field is always associated with dislocations and its interaction with moving magnetic domain walls would

impede the wall motion [22, 25]. This behavior tends to harden the nanocomposite system, because its magnetic anisotropy is greater than that of the bcc phase. However, materials with high magnetic anisotropy usually have high coercivity and hence they are hard to demagnetize. Since the magnetocrystalline anisotropy contributes strongly to the coercive field, it has a great influence on industrial uses of ferromagnetic materials. Moreover, the reduction of crystallite size promotes the formation of single magnetic domains which are more difficult to be oriented due to the presence of the Fe(Si) and Fe(B) phase. This acts as additional obstacles to the magnetic domain wall movement. On the other hand, the decrease of the coercive field can be correlated with the reduction of the grain size and consequently with the deviation of the interatomic distances in the regions interfacial to the crystalline component. It has been shown that the reduction of the coercive field with the reduction of the grain size of the materials up to the range of a few nanometers could be attributed to the presence of superparamagnetic particles [24]. Therefore, the reduction of the coercive field, Hc, in nanocrystalline materials must be clearly distinguished from the superparamagnetic phenomenon where the reduction of Hc is well established in small isolated or weakly coupled particles following thermal excitation [26, 27]. In addition, the variation in saturation magnetization (Ms) with milling time provides additional information on the evolution processes occurring during mechanical alloying. The variation in saturation magnetization Ms with milling time is given in Fig. 7. It can be seen that Ms values increase considerably before 4 h milling for $FeCoNiB_{crystalline}$ and FeCoNiSi with ΔMs~80emu/g, but the difference in values could be correlated with the change in structural parameters due to the alloy process difference caused by the delay of the dissolution of Co and Ni in the Fe network in the presence of Si that the $B_{cristalline}$, while for the $FeCoNiB_{amorphous}$, Ms decreases. After that, the Ms does not present an evolution linked to the processing time but it is strongly dependent on the system compositional evolution. In fact, $FeCoNiB_{crystalline}$ Ms decreases continuously with

milling time after 10h showing for long time milling the lowest saturation of all the alloys. An increase in Ms can be ascribed to the alloying and the diminution of magnetocrystalline anisotropy, which leads to an easier rotation of the magnetic vector. The decrease might be due to the enhanced density of grain boundaries and/or the continuous dissolution of Si and B into Fe lattice. Indeed, the diffusion of metalloids can lead to the introduction of significant plastic deformation and high dislocation densities affecting coercivity, as well. When Si and B are alloyed to Fe and/or Co and Ni, the change of the nearest neighbor configuration leads to the reduction of the magnetic moment per atom and therefore, to the magnetization reduction. This fact can be explained by the interaction between the metallic atoms which are ferromagnetic with Si and B atoms that are non-ferromagnetic in nature [28, 29]. In other way, the fragmentation of the magnetic particles during the milling process leads to a heterogeneous ferromagnetic system where the Fe-rich ferromagnetic grains are separated by Si-rich and B-rich phases. Thus, the coupling between the ferromagnetic grains becomes less effective, giving rise to the observed hardening. For the undoped alloy, Ms increases continuously to a value of 188 emu/g because of the progressive dissolution of the elements Co and Ni, then decreases strongly to regenerate the initial state with an Ms value of 124 emu/g because the grain refinement after 50 h milling.

4. Conclusion

Nanostructured $Fe_{50}Co_{25}Ni_{15}X_{10}$ ($X=B_{amorphous}$, $B_{crystalline}$ and Si) (at.%) powders with semi-hard and soft magnetic properties were prepared by mechanical alloying. The most interesting results of this research are as follows:

- The formation of supersaturated Fe-based solid solutions in nanometer scale is accompanied by an allotropic hcp-Co $\rightarrow$ fcc-Co transformation. The structure of defects produced by high-energy mechanical milling was considered as responsible of these phases transformations.

- The coercivity and magnetization values strongly depend on the structure and magnetically soft materials are only obtained for undoped FeCoNi samples at the end of mechanical milling. In fact, when Si and B are alloyed to FeCoNi, the coercivity increases and the magnetic behavior tends to be semi-hard.

References

1. Suryanarayana, C.: Mechanical alloying and milling. Prog. Mater. Sci. 46, 1 (2001)

2. Koch, C.C.: Top-down synthesis of nanostructured materials: mechanical and thermal processing methods. Rev. Adv. Mater. Sci. 5, 91–99 (2003)

3. Mancier, V., Delplancke, J.L., Delwiche, J., Hubin-Franskin, M.J., Piquer, C., Rebbouh, L., Grandjean, F.: Morphologic, magnetic, and Mossbauer spectral properties of Fe75Co25 nanoparticles prepared by ultrasound-assisted electrochemistry. J. Magn. Magn. Mater. 281, 27–35 (2004)

4. Zhu, J.G.: New heights for hard disk drives. Mater. Today. 6, 22–23 (2003)

5. Sharifati, A., Sharafi, S.: Structure and magnetic properties of mechanically alloyed (Fe70Co30)91Cu9 powder. Mater. Des. 36, 35–40 (2012)

6. Chitsazan, B., Shokrollahi, H., Behvandi, A., Mirzaee, O.: Characterization and magnetic coercivity of nanostructured (Fe50Co50)100-xVx= 0,2,4 powders containing a small amount of Co3V intermetallic obtained by mechanical alloying. Powder Technol. 214, 105–110 (2011)

7. Yuping, D., Yahong, Z., Tongmin, W., Shuchao, G., Xin, L., Xingjun, L.: Evolution study of microstructure and electromagnetic behaviors of Fe–Co–Ni alloy with mechanical alloying. Mater. Sci. Eng. B. 185, 86–93 (2014)

8. Baghbaderani, H.A., Sharafi, S., Chermahini, M.D.: Investigation of nanostructure formation mechanism and magnetic properties in Fe45Co45Ni10 system synthesized by mechanical alloying. Powder Technol. 230, 241–246 (2012)

9. Moumeni, H., Nemamcha, A., Alleg, S., Grenèche, J.M.: Hyperfine interactions and structural features of Fe-44Co-6Mo (wt.%) nanostructured powders. Mater. Chem. Phys. 138, 209–214 (2013)

10. Loureiro, J.M., Costa, B.F.O., Malaman, B., Le Caër, G., Das, S., Amaral, V.S.: Formation stages of bcc (Fe44Co44)Sn12 extended solid solution by mechanical alloying. J. Alloys Compd. 25, 211–218 (2014)

11. Lu, Z., Li, H., Lei, Z., Chang, C., Wang, X., Lu, Z.: The effects of metalloid elements on the nanocrystallization behavior and soft magnetic properties of FeCBSiPCu amorphous alloys. Metals. 8, 283 (2018)

12. Pang, L., Kumar, K.S.: Mater. Sci. Eng. A. 258, 161–166 (1998) 13. Kane, S.N., Gupta, A., Gercsi, Z., Mazaleyrat, F., Varga, L.K.: Magn. Magn. Mater. 292, 447 (2005)

13. Kane, S.N., Gupta, A., Gercsi, Z., Mazaleyrat, F., Varga, L.K.: Magn. Magn. Mater. 292, 447 (2005)

14. Liu, B., Zheng, Y.F., Ruan, L.: Mater. Lett. 65(3), 540–543 (2011) 15. Filho, A.F., Bolfarini, C., Xu, Y., Kiminami, C.S.: Scr. Mater. 42, 213 (2000)

15. Filho, A.F., Bolfarini, C., Xu, Y., Kiminami, C.S.: Scr. Mater. 42, 213 (2000)

16. Yapp, R., Watts, B.E., Leccabue, F.: J. Magn. Magn. Mater. 215, 300 (2000)

17. Lutterotti, L.: MAUD CPD Newsletter. IUCr. 24, (2000)

18. Cardellini, F., Mazzone, G.: Thermal and structural study of the h.c.p.-to-f.c.c. transformation in cobalt. Philos. Mag. 67A(6), 1289–1300 (1993)

19. Sort, J., Nogues, J., Surinach, S., Munoz, J.S., Baro, M.D.: Correlation between stacking fault formation, allotropic phase transformations and magnetic properties of ball-milled cobalt. Mater. Sci. Eng. A. 375–377, 869–873 (2004)

20. Shokrallahi, H.: The magnetic and structural properties of the most important alloys of iron produced by mechanical alloying. Mater. Des. 30, 3374 (2009)

21. Long, J., Ohodnicki, P.R., Laughlin, D.E., McHenry, M.E.: Structural studies of secondary crystallization products of the Fe23B6-type in a nanocrystalline FeCoB-based alloy. J. Appl. Phys. 101, 09N114 (2007)

22. Souilah, S., Alleg, S., Djebbari, C., Bensalema, R., Sunol, J.J.: Magnetic and microstructural properties of the mechanically alloyed Fe57Co21Nb7B15 powder mixture. Mater. Chem. Phys. 132, 766–772 (2012)

23. Bensalem, R., Alleg, S., Younes, A., Souilah, S., Azzaza, S., Sunol,J.J.: Al-Azhar Univ. Eng. J. JAUES. 3(13), 83–92 (2008)

24. Herzer, G.: Grain size dependence of coercivity and permeability in nanocrystalline ferromagnets. IEEE Trans. Magn. 26, 13977 (1990)

25. Delshad Chermahini, M., Sharafi, S., Shokrollahi, H., Zandrahimi,M., Shafyei, A.: The evolution of heating rate on the microstructural and magnetic properties of milled nanostructured Fe1-xCox(x =0.2, 0.3, 0.4, 0.5 and 0.7) powder. J. Alloys Compd. 484, 54–58 (2009)

26. Luborsky, F.E.: Development of elongated particle magnets. J. Appl. Phys. 32, S171 (1961)

27. Kneller, E.: Fine particle theory. In: Berkowitz, A.E., Kneller, E. (eds.) Magnetism and Metallurgy, vol. 1, pp. 365–471. Academic Press, New York (1969)

28. Abdellaoui, M., Djega-Mariadassou, C., Gaffet, E.: Structural study of Fe-Si nanostructured materials. J. Alloys Compd. 259, 241 (1997)

29. Bensebaa, N., Loudjani, N., Alleg, S., Dekhil, L., Suñol, J.J., Al Sae, M., Bououdina, M.: XRD analysis and magnetic properties of nanocrystalline Ni20Co80 alloys. J. Magn. Magn. Mater. 323, 3063–3070 (2011)

Figures captions

Fig. 1. Morphological evolution of the powder particles of the $Fe_{50}Co_{25}Ni_{25}$, $Fe_{50}Co_{25}Ni_{15}B_{10(amorphous)}$, $Fe_{50}Co_{25}Ni_{15}B_{10(crystalline)}$ and $Fe_{50}Co_{25}Ni_{15}Si_{10(amorphous)}$, before milling (a, b, c and d, repectivety) and after 50 h (a1, b1, c1 and d1, respectively) and 100h (a2, b2, c2 and d2), respectively.

Fig. 2. XRD patterns of powders of the (a) $Fe_{50}Co_{25}Ni_{25}$, (b) $Fe_{50}Co_{25}Ni_{15}B_{10(amorphous)}$, (c) $Fe_{50}Co_{25}Ni_{15}B_{10(crystalline)}$ and (d) $Fe_{50}Co_{25}Ni_{15}Si_{10}$ collected at different milling times.

Fig. 3. Lattice parameter variations of of the $Fe_{50}Co_{25}Ni_{25}$, $Fe_{50}Co_{25}Ni_{15}B_{10(amorphous)}$, $Fe_{50}Co_{25}Ni_{15}B_{10(crystalline)}$ and $Fe_{50}Co_{25}Ni_{15}Si_{10}$ against milling time.

Fig. 4. Evolution of microstructural parameters versus milling time: (a) Crystallite size and (b) lattice strains of the $Fe_{50}Co_{25}Ni_{25}$, $Fe_{50}Co_{25}Ni_{15}B_{10(amorphous)}$, $Fe_{50}Co_{25}Ni_{15}B_{10(crystalline)}$ and $Fe_{50}Co_{25}Ni_{15}Si_{10}$ against milling time.

Fig. 5. Typical hysteresis loops dependence on selected milling time of the of the $Fe_{50}Co_{25}Ni_{25}$, $Fe_{50}Co_{25}Ni_{15}B_{10(amorphous)}$, $Fe_{50}Co_{25}Ni_{15}B_{10(crystalline)}$ and $Fe_{50}Co_{25}Ni_{15}Si_{10}$ powders, at T=300 K.

Fig. 6. Coercive field Hc dependence on milling time of the $Fe_{50}Co_{25}Ni_{25}$, $Fe_{50}Co_{25}Ni_{15}B_{10(amorphous)}$, $Fe_{50}Co_{25}Ni_{15}B_{10(crystalline)}$ and $Fe_{50}Co_{25}Ni_{15}Si_{10}$ powders.

Fig. 7. Saturation magnetization dependence on milling time of the $Fe_{50}Co_{25}Ni_{25}$, $Fe_{50}Co_{25}Ni_{15}B_{10(amorphous)}$, $Fe_{50}Co_{25}Ni_{15}B_{10(crystalline)}$ and $Fe_{50}Co_{25}Ni_{15}Si_{10}$ powders.

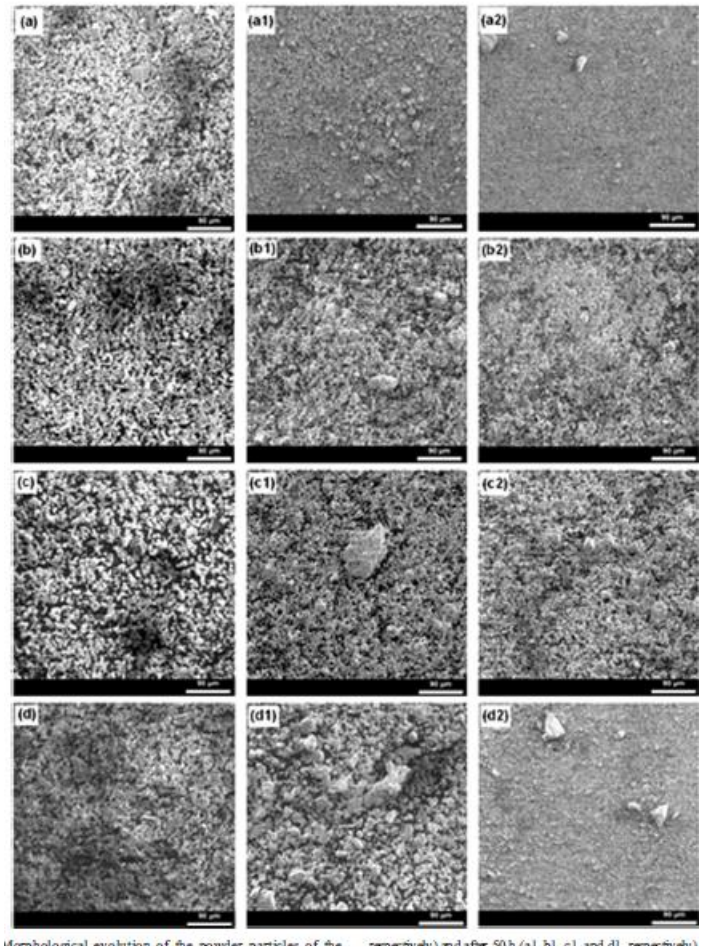

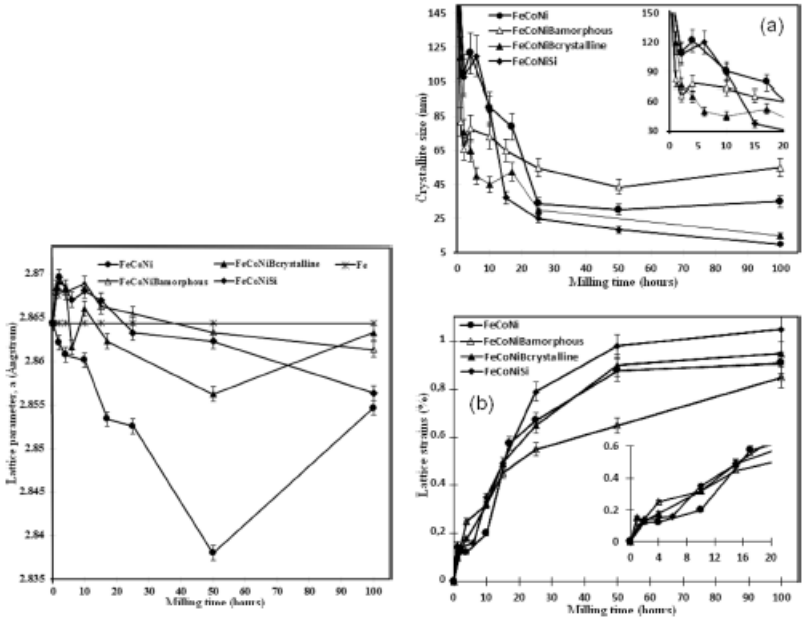

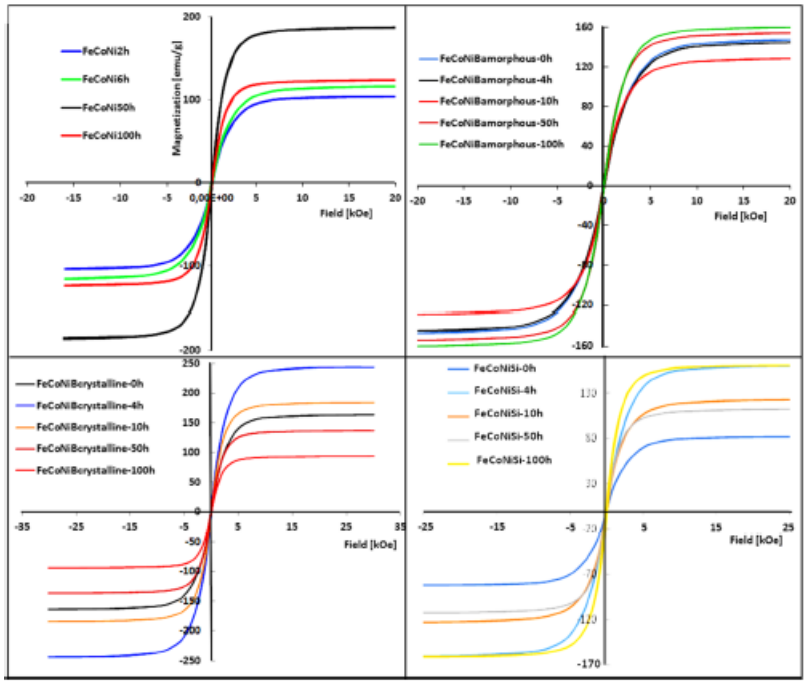
FeCoNi2h
FeCoNi6h
FeCoNi50h
FeCoNi100h
Magnetization [emu/g]
Field [kOe]
FeCoNiBamorphous-0h
FeCoNiBamorphous-4h
FeCoNiBamorphous-10h
FeCoNiBamorphous-50h
FeCoNiBamorphous-100h
Field [kOe]
FeCoNiBcrystalline-0h
FeCoNiBcrystalline-4h
FeCoNiBcrystalline-10h
FeCoNiBcrystalline-50h
FeCoNiBcrystalline-100h
Field [kOe]
FeCoNiSi-0h
FeCoNiSi-4h
FeCoNiSi-10h
FeCoNiSi-50h
FeCoNiSi-100h
Field [kOe]

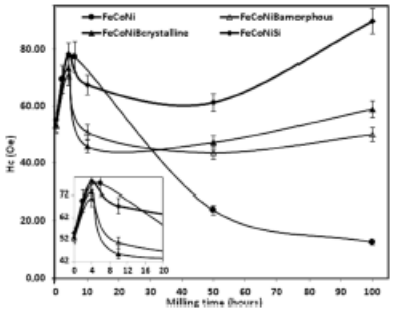
FeCoNi
FeCoNiBamorphous
FeCoNiBcrystalline
FeCoNiSi
Hc (Oe)
Milling time (hours)

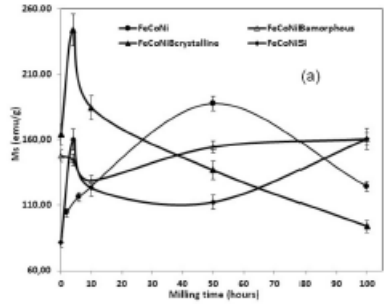
FeCoNi
FeCoNiBamorphous
FeCoNiBcrystalline
FeCoNiSi
(a)
Ms (emu/g)
Milling time (hours)

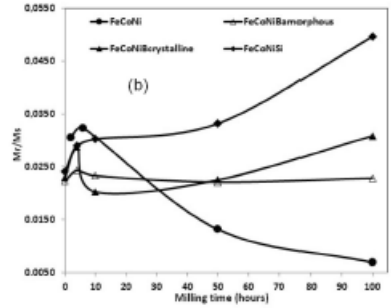
FeCoNi
FeCoNiBamorphous
FeCoNiBcrystalline
FeCoNiSi
(b)
Mr/Ms
Milling time (hours)